atmosphere

MDPI

Article

An Analysis of Regional Ozone Pollution Generation and Intercity Transport Characteristics in the Yangtze River Delta

Yu Cao [1,2], Jinghui Ma [1,2,3,*], Xiaoyi Wang [4] and Juanjuan Bian [1]

[1] Shanghai Typhoon Institute, Shanghai Meteorological Service, Shanghai 200030, China; liushuicaoyu@163.com (Y.C.); bianandbian123@163.com (J.B.)
[2] Shanghai Key Laboratory of Meteorology and Health, Shanghai Meteorological Service, Shanghai 200030, China
[3] Department of Atmospheric and Oceanic Sciences, Institute of Atmospheric Sciences, Fudan University, Shanghai 200438, China
[4] Plateau Atmosphere and Environment Key Laboratory of Sichuan Province, College of Atmospheric Science, Chengdu University of Information Technology, Chengdu 610225, China
* Correspondence: 18918206605@163.com; Tel.: +86-21-54896867

Abstract: Understanding the relative contributions of regional transport and local generation, alongside the nonlinear relationships between ozone (O_3) and its precursors, is essential for formulating effective O_3 pollution control strategies. The Yangtze River Delta region experiences pronounced O_3 pollution transmission between cities, with pollutants capable of spreading hundreds of kilometers downwind under varying wind, temperature, and humidity conditions. However, the distributional characteristics of regional O_3 pollution transmission across different cities within this area remain unclear. This study applies the Texas Commission on Environmental Quality method to assess the spatial distribution of regional background and locally generated ozone concentrations, while using a composite analysis to examine the wind and temperature field characteristics during typical years of high ozone transport and local generation episodes. The results indicate that ozone concentrations across regions are strongly influenced by local wind anomalies, with elevated temperatures correlating with high O_3 concentrations. Furthermore, an algorithm based on observed O_3 concentrations and ground-level wind data was developed to quantify pollution transport rates more accurately, addressing uncertainties in pollutant transport dynamics due to variable wind fields and identifying "false" potential source areas. The findings reveal that intercity transport within the Yangtze River Delta contributes 45.2–65.1% to regional O_3 levels, exceeding local generation in impact. Shanghai experiences the highest transmission influence (over 50%), while Zhejiang Province shows a dominant local generation influence (below 20%). In Anhui Province, O_3 concentrations are notably high, with significant internal transport and substantial transmission to Jiangsu Province. This study offers valuable insights into the pathways, traceability, and three-dimensional wind field characteristics of O_3 pollution across cities in the Yangtze River Delta, elucidating the dynamic mechanisms necessary for mitigating O_3 pollution transmission in diverse urban settings.

Keywords: wind field; transportation; the Texas commission on environmental quality (TCEQ) method

Academic Editors: Qiaoli Wang and Yao Shen

Received: 2 December 2024
Revised: 13 January 2025
Accepted: 21 January 2025
Published: 31 January 2025

Citation: Cao, Y.; Ma, J.; Wang, X.; Bian, J. An Analysis of Regional Ozone Pollution Generation and Intercity Transport Characteristics in the Yangtze River Delta. *Atmosphere* **2025**, *16*, 158. https://doi.org/10.3390/atmos16020158

1. Introduction

Ozone (O_3) has recently emerged as a major air pollutant in China, particularly in key industrial and densely populated regions [1,2]. Since 2015, successive rounds of environmental protection action plans have notably improved the air quality across China's three major regions. By 2021, annual average concentrations of $PM_{2.5}$, PM_{10}, NO_2, and SO_2 in the Yangtze River Delta decreased by 8.2%, 5.0%, 3.4%, and 17%, respectively—reductions more substantial than those observed in the Pearl River Delta but less pronounced compared to Beijing–Tianjin–Hebei. Unlike these conventional pollutants, however, the maximum 8 h ozone concentration and atmospheric oxidation indicator (Ox) showed consistent increases in all three regions. Specifically, the annual increases in O_3–8 h and Ox in the Yangtze River Delta were 1.4% and 1.3%, respectively, surpassing those in Beijing–Tianjin–Hebei but were lower than in the Pearl River Delta [3]. Additionally, the number of days when O_3 was the primary pollutant has markedly risen, and by 2021, these days exceeded those when $PM_{2.5}$ was dominant. This trend indicates a substantial deterioration in O_3 pollution, shifting the pollution profile in the Yangtze River Delta to a dual focus on $PM_{2.5}$ and O_3 pollution, with O_3 exhibiting a distinct upward trend [4,5]. Consequently, O_3 now represents a critical factor constraining air quality improvements. O_3 concentrations are influenced not only by photochemical reactions involving locally emitted precursors but also by the transport of O_3 or O_3 precursors generated in surrounding regions. Therefore, a detailed investigation into the transport characteristics and sources of O_3 pollution in the Yangtze River Delta is vital for enabling decision-makers to devise precise and effective control strategies [6–9].

Wind fields are instrumental in shaping atmospheric pollutant transport dynamics, with their three-dimensional structure impacting both horizontal and vertical dispersion patterns related to O_3 pollution. Strong winds generally facilitate pollutant dispersion, reducing concentration levels, while weak winds lead to pollutant accumulation, resulting in a negative correlation between wind speed and pollutant concentration [10,11]. Consistently low wind speeds contribute to large-scale O_3 pollution events with integral or bicentric spatial distributions, aligning with atmospheric circulation analysis findings. Low wind speeds extend reaction times for ozone precursors, reducing dispersion and sedimentation, which collectively heightens O_3 levels. Although strong winds assist in dispersing local pollutants, they may also transport high-concentration O_3 pollutants downstream, potentially raising contamination levels in downwind areas [12,13].

Current quantitative methods for analyzing regional O_3 transport contributions primarily include the backward trajectory method and chemical weather model analysis. The backward trajectory model efficiently determines pollutant arrival times and transport speeds, frequently in conjunction with a cluster analysis, trajectory statistics, and other approaches to identify pollutant pathways and potential source areas [14–18]. For example, Nzotungicimpaye et al. [19] used backward trajectory analysis to establish that industrial plateau emissions were the main O_3 source in Cape Town, identifying four principal transmission paths, which notably deteriorate air quality along the northeastern and southern coastal routes. Building on trajectory analysis, Vellingiri et al. [20] applied potential source contribution function analysis to determine that heightened NO_2 levels in Seoul, South Korea, were primarily driven by emissions from North China and local sources, while O_3 originated mainly from oceanic and mountainous regions in China and Japan. Chemical weather model analyses, which include sensitivity testing, adjoint analysis, and tracer analysis, provide further insights. Xue et al. [21] applied an OBM (observation-based model) model to evaluate four downwind sites across major Chinese cities—Beijing, Shanghai, Guangzhou, and Lanzhou—concluding that Beijing's downwind areas were predominantly influenced by regional O_3 transmission, while those in Shanghai,

Guangzhou, and Lanzhou were largely affected by local O_3 generation. During source region identification, these statistical approaches utilize pollutant concentration monitoring at receptor sites as a key parameter. Although computationally efficient and straightforward, this approach may inadequately represent actual pollutant concentrations within each grid along the trajectory path, posing the risk of identifying "false" potential source regions and thus compromising the accuracy of transmission characteristics.

Previous studies [22,23] have highlighted significant inter-regional O_3 transport within the Yangtze River Delta, in contrast to the predominantly local accumulation observed in the Pearl River Delta and Beijing–Tianjin–Hebei regions. Understanding the contributions of both regional transport and local generation forms the basis for implementing coordinated regional control measures. This study utilizes the Texas Commission on Environmental Quality (TCEQ) methodology to estimate regional background levels and local distribution patterns of O_3 concentrations, further analyzing temperature field characteristics under two representative annual wind patterns. Additionally, an algorithm was developed based on empirical data to quantify air pollutant transport rates effectively during May–June from 2015 to 2020, focusing on the Category 5 classification for regional O_3 pollution distribution types. Evaluating air mass transport paths◎contribution rates to O_3 pollution across four key cities provides insights essential for designing rational emission reduction strategies to mitigate O_3 contamination across these regions.

2. Data and Methods

2.1. Data Source

O_3 concentration data for the Yangtze River Delta (YRD) region, spanning January 2015–December 2020, were obtained from the National Urban Air Quality Real-Time Release Platform (http://113.108.142.147:20035/emcpublish/ (accessed on 2 January 2024)). This dataset provides hourly O_3 concentration readings from 256 national monitoring stations, distributed across Anhui, Jiangsu, Shanghai, and Zhejiang, with 73, 114, 10, and 59 monitoring sites, respectively. The geographic distribution of the major cities within the YRD is shown in Figure 1a.

Ground meteorological observation data were sourced from the China Meteorological Administration (https://weather.cma.cn/ (accessed on 3 January 2024)) and include hourly records of the temperature, relative humidity, and horizontal wind speed and direction from 228 regional meteorological stations across the YRD. The spatial distribution of these meteorological stations is illustrated in Figure 1b. Atmospheric circulation data were derived from the ERA-5 reanalysis dataset provided by the American Institute for Environmental Studies [24], covering a spatial range of 20–50° N and 100–130° E, with a horizontal resolution of 1° × 1° and four daily time points (UTC 00:00, 06:00, 12:00, and 18:00). This dataset includes sea level pressure and 10 m horizontal wind components (U and V). The validity of the O_3 observation and meteorological data for each YRD province is summarized in Table 1.

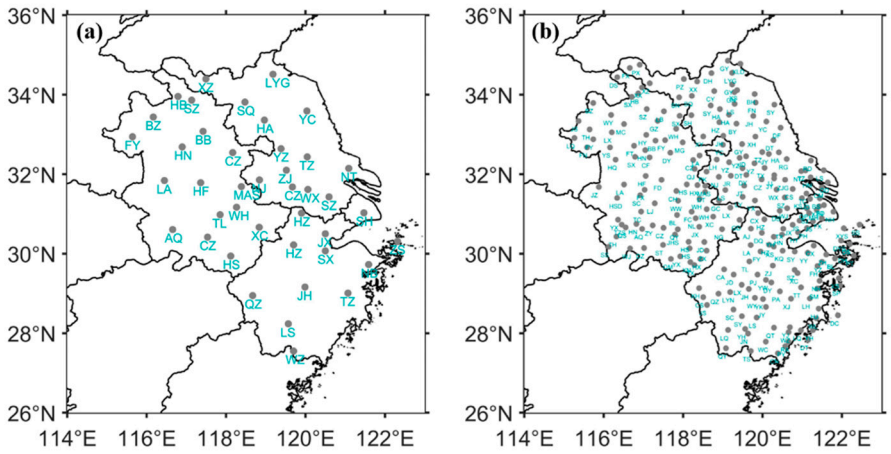

Figure 1. Distribution map of meteorological stations in (**a**) 41 cities and (**b**) 241 regions within the YRD region.

Table 1. Validity of O_3 observation and meteorological data in YRD provinces.

Provincial	Observation Station Number	Data Quantity	Data Efficiency
Anhui	73	1,301,736	97%
Jiangsu	114	2,032,848	98%
Zhejiang	59	1,052,088	98%
Shanghai	10	178,320	99%

2.2. Methods

2.2.1. TCEQ Method

The TCEQ method, initially developed by the Texas Commission on Environmental Quality in the United States, was later refined by Nielsen-Gammon et al. [25], who introduced a more automated approach for analyzing the daily maximum 8 h average ozone (DMA8–O_3). This method leverages a robust air quality monitoring network that ensures comprehensive spatial coverage, accounting for variations in wind direction. It is assumed that regardless of wind direction changes, at least one monitoring station will consistently capture upwind regional air mass inputs, while other stations may reflect localized photochemical processes to varying extents. Consequently, the minimum DMA8–O_3 value recorded among all monitoring stations is used as an indicator of regional background ozone levels, while the maximum DMA8–O_3 value denotes peak ozone concentrations within the area. The difference between these maximum and minimum values quantifies the capacity of local precursor emissions to produce ozone through photochemical reactions, with the resulting value representing locally generated ozone.

$$LO_3 = DAO8_{max} - DAO8_{min} \quad (1)$$

In Formula (1), LO_3 represents the local generation of O_3. $DAO8_{max}$ is the highest daily 8 h average O_3 concentration recorded across all monitoring sites in the region, while $DAO8_{min}$ is the lowest daily 8 h average O_3 concentration from the filtered sites within the same area. This analysis encompasses data from forty-three cities within the study region.

2.2.2. O_3 Transport Rate Algorithm

To address uncertainties in pollutant transport between regions, arising from wind field variability and "false" source areas identified through HYSPLIT® methodology [26,27], this study applied a robust O_3 transport rate algorithm (TOR) based on observed

O_3 concentrations and surface wind field data. The TOR computational framework involves three primary steps:

(1) Quantitative modeling based on hourly O_3 and meteorological parameter observations.
(2) Backward trajectory calculation to model observed O_3 transport paths.
(3) Clustering analysis to identify key transport channels and to quantify intercity transport contributions across five defined spatial categories.

To illustrate the TOR modeling process, we considered a hypothetical transport event from zone i to zone j. To model such a process from district i to j, the first step involves estimating the probability of pollutant transport from zone i to zone j (see Figure 2A). Following Seinfeld et al.'s air packet approach [28], we employ a sampling technique to simulate pollutant transport paths accurately (illustrated in Figure 2C). Specifically, air parcels, representing air pollutants, are released near the district i at the timestamp t in a simulation. The locations of these air parcels are updated iteratively based on the meteorological conditions, including the wind speed and direction (Figure 2B), until the distance between the air parcel and the district j falls under $d_e = 20$ km or the time limit is exceeded (72 h). Inspired by HYSPLIT's approach [26,27], we calculated each air packet's position at time t using the following equation:

$$L(\Delta t + t) = L(t) + \overrightarrow{v_t} \times \Delta t$$

$$\overrightarrow{v_t} = \frac{\sum_{m \epsilon M}(d_n - d_m) \times \overrightarrow{v_{m,t}}}{\sum_{m \epsilon M}(d_n - d_m)} \quad (2)$$

In this context, $\overrightarrow{v_t}$ represents the air packet's speed at the location L(t) at the timestamp t, while M denotes a set of nearby meteorological observation stations, where the distance between each station and the air parcel is measured to be d_m, within the given distance threshold $d_n = 20$ km. Thus, the closer an air pollutant concentration observation station is to the air packet, the greater its contribution is to the wind vector from that meteorological station ($\overrightarrow{v_{m,t}}$). Hereafter, we denote the number of the air parcels that reached the district j as s_r and the travel time of the k-th air parcels as tt_k, $k < s_r$. Based on this, we define the transmission probability P_{ijt} for the observed pollutant concentration from the initial position i to the target position j at timestamp t, as shown in Formula (3):

$$P_{ijt} = \frac{S_r}{S} \quad (3)$$

where S_r represents the subset of air packets that successfully reach the target area, and S denotes the total number of packets released from the source.

The average transport time was averaged to generate the final results. Figure 2C,D provide an example of calculating transport probability by sampling air packets, from which the transport trajectory for each pollution event is derived (Figure 3d). Each transport trajectory comprises two nodes, representing positions i and j, connected by a directional edge indicating the transport direction. In this framework, each node n includes additional parameters: the timestamp n.t and the observed pollution concentration n.c. at time n.t. Furthermore, additional information is computed along each directional edge e_{ij}: (a) the transport duration for each instance is denoted by e_{ij}.tt; (b) e_{ij}.p is the estimated transport probability, indicating the contribution factor, or the proportion of pollutants transported from the origin to the destination; (c) thus, we can calculate the quantity of transported pollutants as $e_{ij}.tc = e_{ij}.p \times n_j.c$; (d) finally, we define an impact factor e_{ij}.a = e_{ij}.tc/n_j.c, which represents the ratio of pollutants received at the endpoint

relative to those originating from the start point. If comprehensive testing results indicate $e_{ij}.\mathrm{tc} < 30$, pollutant transportation is deemed negligible.

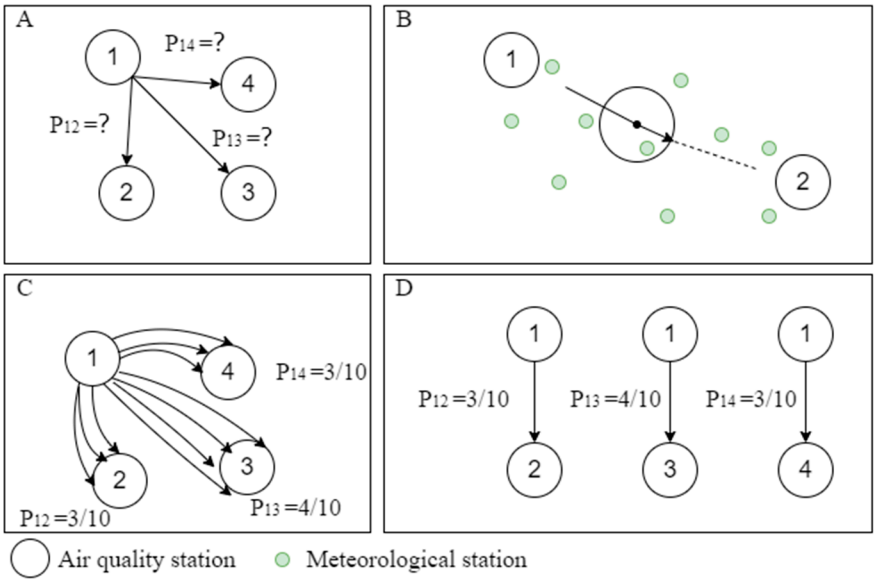

Figure 2. (**A**) Probability of air pollutant transport from Source 1; (**B**) iterative refinement of air mass position; (**C**) quantitative sampling methodologies; (**D**) real-time acquisition of individual transport trajectories.

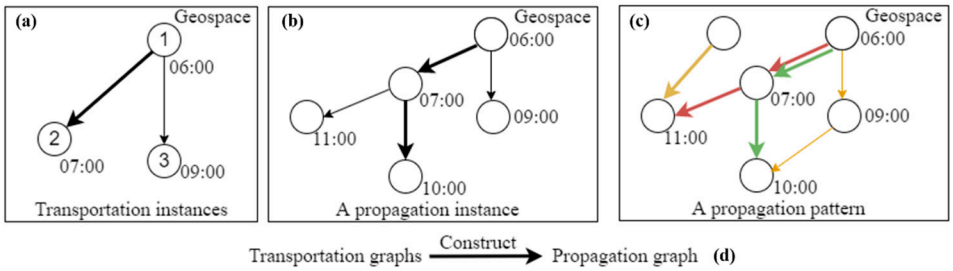

Figure 3. Flowchart of the primary pollutant transport calculation process: (**a**) two distinct transport pathways between points 1 and 2 (major pathway) and between points 1 and 3 (minor pathway); (**b**) a transport process with four concurrent pathways; (**c**) transmission modules defined from four identified transmission tracks, each coded by color; (**d**) a single transport process trajectory composed of multiple individual transport instances.

In the context of regional O_3 pollution transport within the YRD, O_3 concentration and wind vector fields demonstrate concurrent temporal and spatial variations. Compared to traditional backward trajectory models and other methodologies [29], this approach offers two distinct advantages. First, by incorporating measured O_3 concentrations and meteorological observation data, along with an hourly correction algorithm for wind vector fields, this method departs from conventional models by providing a more accurate calculation of regional pollutant transmission trajectories. This enhanced approach enables a finer depiction of the pollution transmission process. Second, the iterative adjustment of the wind vector field on a grid-by-grid, hourly basis ensures that the model closely reflects real-time transmission dynamics, as wind vector fluctuations significantly impact pollutant transport. This method models the entire transmission pathway comprehensively, tracking pollutant movement from an origin (zone i) to a target destination (zone j) with time-stamped positions, integrating each step into the overall transport process.

Finally, clustering techniques were applied to evaluate the frequency of different transmission pathways and to quantify intercity transport contributions. Notably, current calculations of O_3-polluted air mass transport paths at specific times do not include secondary effects from previous emissions or cumulative concentrations along these pathways, maintaining a focused assessment of direct pollutant transport dynamics.

3. Results

This study examines the background concentration of O_3 and the distribution of its generation contributions across the YRD, while identifying key meteorological factors influencing O_3 transmission. Using the regional O_3 pollution classification by Cao et al. [30], four major cities were selected to assess O_3 transmission characteristics across five types of regional O_3 processes.

3.1. Estimation of Regional Background Ozone and Locally Generated Concentrations

Ozone concentration at any given location can be viewed as the sum of regional background ozone levels and locally generated photochemical ozone concentrations. Regional background ozone refers to the concentration within the study area, assuming no local precursor emissions, typically simulated by deactivating precursor emissions in air quality models [31–33]. In this study, regional background ozone specifically represents the concentration of ozone transported from external sources into the target area. The TCEQ methodology, as developed by Nielsen-Gammon et al. [25], was applied to determine background O_3 concentrations at monitoring stations throughout the YRD. The results indicate that from May to September, the average background O_3 concentration in this region was 78.7 $\mu g \cdot m^{-3}$. Spatial distribution patterns are presented in Figure 4a, highlighting that the areas surrounding Taihu Lake show the highest background concentrations; Huzhou recorded a peak level at 108.7 $\mu g \cdot m^{-3}$, followed by Hangzhou, Wuxi, Changzhou, Zhenjiang, and Yangzhou, while Huangshan registered the lowest value at 48.2 $\mu g \cdot m^{-3}$.

Daily estimations of locally generated ozone concentrations were derived from the difference between DMA8–O_3 readings and regional background levels recorded at each monitoring station. During the period from May through September, the average generated O_3 concentration in the YRD was approximately 44.9 $\mu g \cdot m^{-3}$, with local contributions accounting for about 36.3% of the total ozone levels (encompassing both regional background and locally generated components). Figure 4b illustrates the spatial distribution of locally generated O_3 across the region, showing significant O_3 generation in parts of Jiangsu Province, as well as Northern Anhui and Northern Zhejiang. These high ozone areas also have higher volatile organic compounds (VOCs) and NOx emissions from industrial activities, but whether there is a correlation between these two factors remains to be studied (see Figure 5). Additionally, geographical factors play a role; inland cities distant from coastal regions show enhanced ozone generation potential due to favorable conditions for ozone formation.

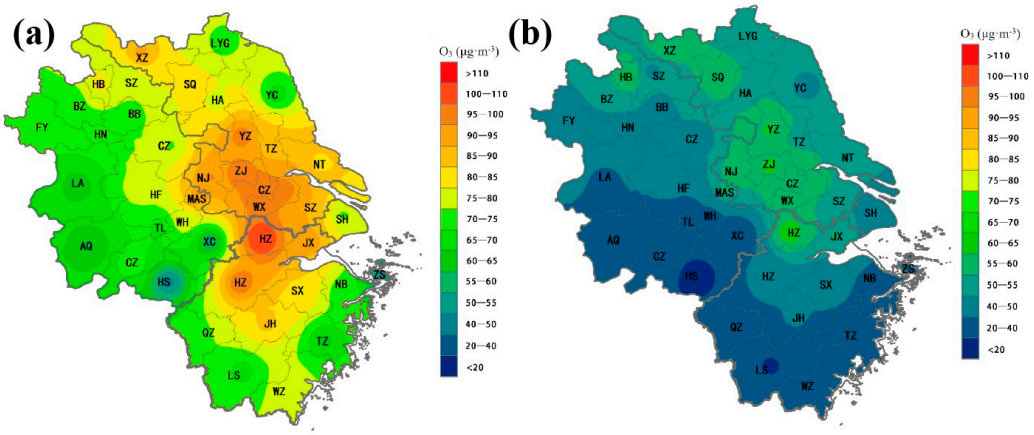

Figure 4. (**a**) Regional background concentration of O_3 and (**b**) spatial distribution of O_3 generation in the YRD region from May to September, as determined using the TCEQ method.

The TCEQ methodology was applied to estimate daily regional background and local ozone concentrations, as well as to calculate annual mean values (see Figure 6). From 2015 to 2022, both background and locally generated ozone concentrations in the YRD region demonstrated a gradual upward trend, highlighting a worsening ozone pollution scenario with annual fluctuations. Between 2015 and 2017, background ozone levels rose significantly, while locally generated ozone increased at a slower rate, suggesting that transboundary transport contributed more substantially to the overall ozone levels within the region. From 2017 to 2019, background concentrations leveled off, while local ozone production rebounded after a notable decline in 2018. This pattern implies that the reduction in ozone levels during 2018 was primarily due to decreased local production. Between 2019 and 2021, background concentrations declined rapidly, while locally generated ozone initially decreased before increasing again. The rapid decline of background ozone concentrations could probably be connected with the lockdown during COVID-19. In 2022, both the background and local ozone concentrations spiked, attributed to intense ozone formation linked to one of the most severe prolonged dry heat events recorded since monitoring systems were established in the Yangtze River Basin.

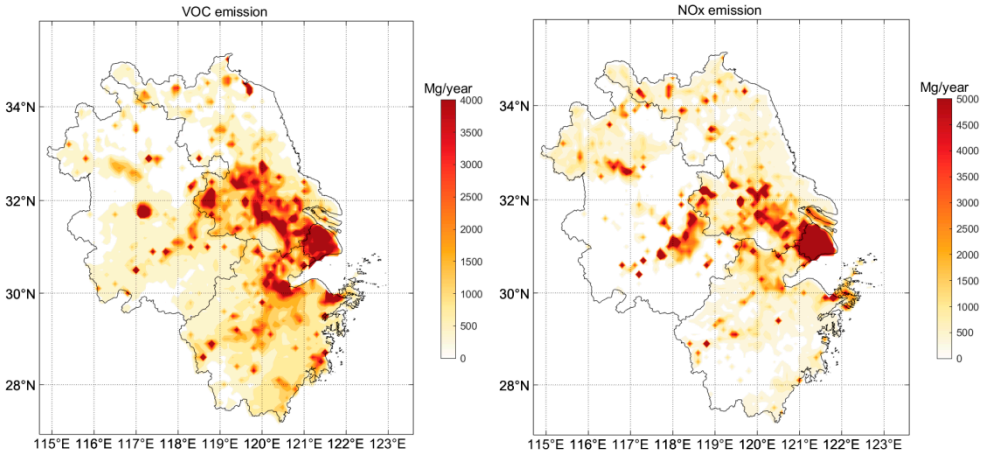

Figure 5. Spatial distribution of O_3 precursor emissions in the YRD.

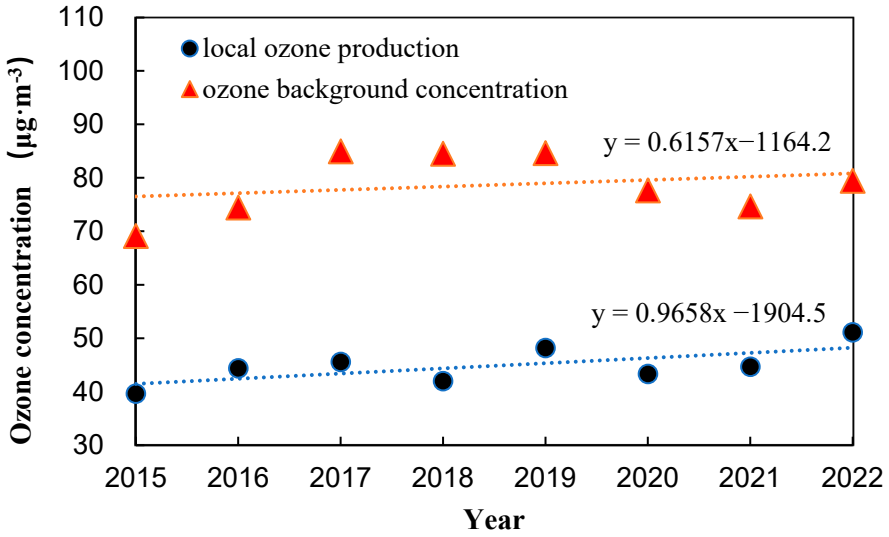

Figure 6. Annual changes of O_3 generation and local concentration in the YRD region.

Data from years with elevated background ozone concentrations (2017, 2018, and 2019) were selected for a composite analysis. The maximum 8 h daily average wind field and ozone concentration (MDA8) anomaly values were calculated as the difference between the May to September averages of each typical year and those of the same period from 2015 to 2022 (Figure 7a). In these years, marked by strong ozone transport characteristics, Shanghai shows a positive O_3 anomaly, accompanied by notably stronger southwest or west winds, indicating that O_3 levels in Shanghai are primarily influenced by transport from western and southwestern regions. Wind convergence is prominent in Huaibei, Suzhou, Chuzhou, Bozhou in Northern Anhui, and Xuzhou in Northern Jiangsu, facilitating elevated O_3 concentrations across Anhui and Northwest Jiangsu. Significant ozone anomaly centers appear in Hefei, Ma@anshan, Wuhu, and Nanjing, correlating closely with the convergence of southwesterly winds in these areas. The western and southern parts of this region, characterized by mountainous terrain and high forest coverage, see VOC emissions from biogenic sources transported into the area under the influence of southwesterly winds, further raising O_3 levels. Apart from a negative O_3 anomaly observed in Southeastern Zhejiang Province, most other areas show positive O_3 anomalies associated with prevailing southwest winds.

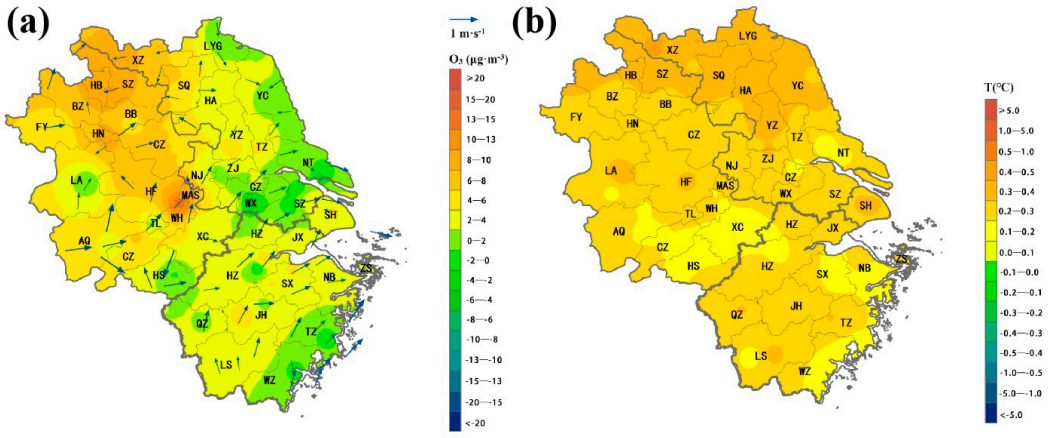

Figure 7. (**a**) Composite wind field anomaly from May to September for 2017, 2018, and 2019, alongside the 8 h average O_3 concentration anomaly; (**b**) composite temperature anomaly observed in 2016, 2017, 2019, and 2022.

For a composite analysis of local ozone generation during peak years (2016, 2017, 2021, and 2022), data from May to September were analyzed alongside average daily temperatures for these months, compared against averages from the same period between 2015 and 2022 (Figure 7b). Years with increased local ozone production across the YRD region displayed consistently elevated temperatures. Specifically, temperatures exceeded +0.3 °C in Shanghai, Central/Northern Jiangsu, and Northern Anhui (including Hefei), with some areas surpassing +0.4 °C. The spatial distribution of these temperature anomalies closely aligns with localized ozone generation patterns identified using the TCEQ methodology (Figure 4b), underscoring the positive effect of higher temperatures on ozone formation, consistent with previous research findings.

3.2. Transportation Routes and Contribution Rates of Key Cities

Ozone transport dynamics among cities in the YRD region are notably significant. To analyze intercity transport patterns across different pollution types, we integrated five distinct ozone concentration distribution categories, as outlined by Cao et al. [30]. Using the TOR (Transport Rate) method, we calculated 72 h transport trajectories and transmission rates for these distribution types across four major cities—Hefei, Nanjing, Shanghai, and Hangzhou (see Figure 8). The results reveal that intercity transport contributions within the YRD range from 45.2% to 65.1%, surpassing contributions from local ozone generation, consistent with previous findings [34]. As shown in Figure 8, the primary source direction of O_3 pollutants is less correlated with the distribution type; instead, the pollution distribution type primarily dictates both initial transport mechanisms and intercity transport proportions. For example, in Hefei, ozone concentrations are predominantly influenced by southerly transport routes, especially along the Anqing–Chizhou–Hefei corridor, contributing 32.3–42.1% of Hefei's ozone levels. Nanjing's ozone is chiefly affected by external provincial transports, with the most substantial northwestward flow occurring along the Huaibei–Bengbu–Chuzhou–Nanjing route, contributing 28.2–39.9%. In contrast, over half of Shanghai's ozone originates from areas outside the city, predominantly from the west–southwest direction, with significant transport occurring along the Wuhu–Xuancheng–Huzhou pathway through the Taihu Basin into Shanghai (transport contribution: 41.8–51.2%). Short-distance transfers from the Taihu Basin directly into Shanghai are also notable, particularly within bicentric and inland distribution types (contribution: 36.2–47.2%). The Taihu Basin thus emerges as a crucial ozone generation zone within the YRD (refer to Figure 4b). Among these four key cities, Hangzhou shows the least influence from intercity O_3 transport. Its primary transport channel is the Huaian–Yangzhou–Circum–Taihu Basin–Huzhou–Hangzhou route, with a transport contribution ranging from 9.9% to 24.5%. Similar to Shanghai, the Taihu Basin area serves as an essential O_3 source for Hangzhou, indicating that southern YRD cities are significantly impacted by polluted air masses around Taihu Lake. Conversely, central and northern cities benefit from trans-regional ozone transport from Northern Jiangsu Province and North China.

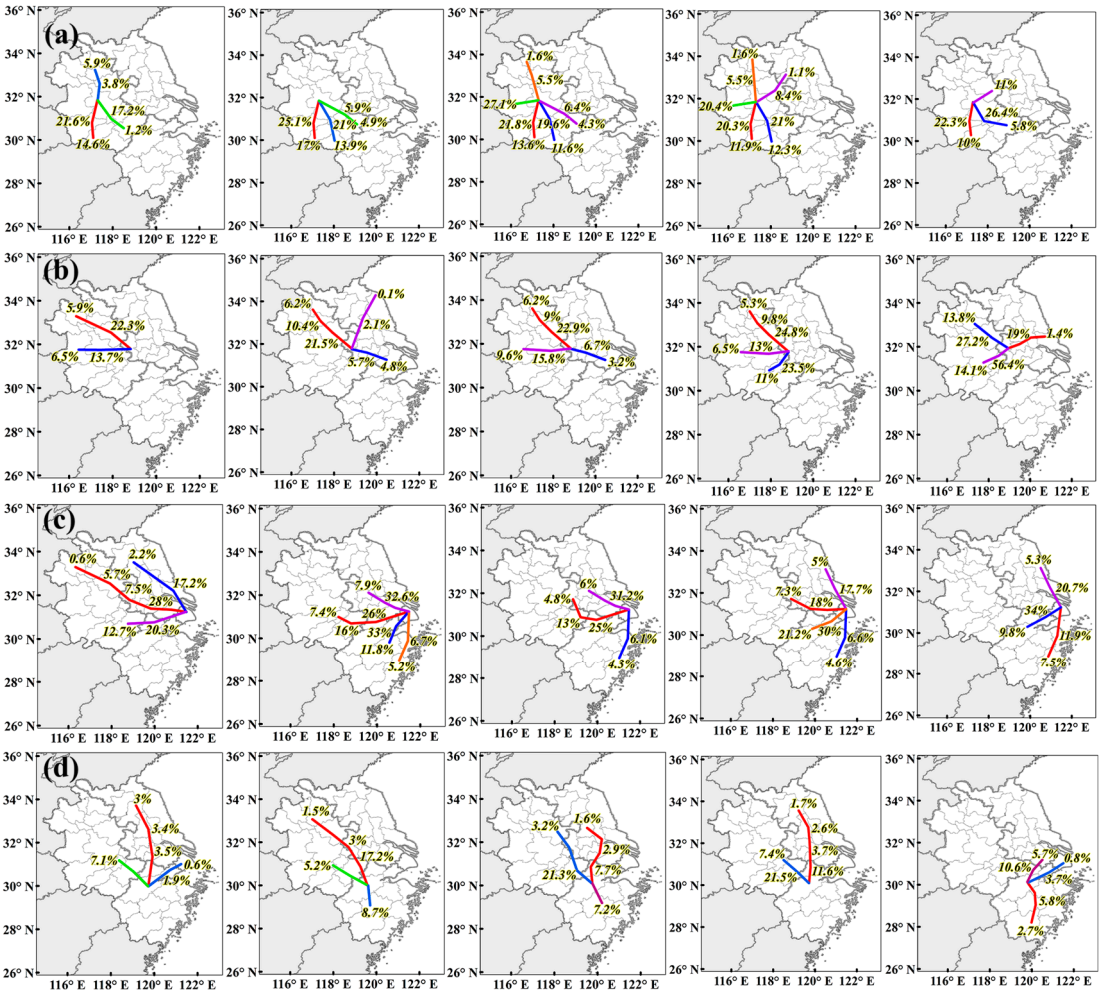

Figure 8. Main trajectory and source contribution characteristics of O_3 pollution transport in the Class 5 YRD region for 72 h: (**a**) Hefei; (**b**) Nanjing; (**c**) Shanghai; (**d**) Hangzhou.

4. Discussion and Summary

This study outlines the spatial distribution characteristics of elevated ozone (O_3) concentrations in the YRD region, focusing on the distribution patterns of background ozone levels and locally generated photochemical ozone. It further explores meteorological field variations between years characterized by significant transport and those driven by local ozone generation. By analyzing five types of high-concentration ozone distributions, this research identifies the main transport channels and their contributions to ozone levels in four key cities from a three-dimensional wind field perspective. This study leads to three primary conclusions:

(1) The average O_3 concentration in the YRD from May to September is approximately 44.9 μg·m^{-3}, with local generation accounting for about 36.3% of the total O_3 (encompassing both regional background and locally generated concentrations). High ozone concentrations are prevalent in most areas of Jiangsu, Northern Anhui, and Northern Zhejiang, with the area around Taihu Lake exhibiting the highest background O_3 levels in the region. Notably, Huzhou records an exceptionally high background concentration of 108.7 μg·m^{-3}.

(2) From 2015 to 2022, background and local O_3 generation rates across the YRD gradually increased. In particular, 2022—a year marked by one of the most severe complex dry heat events since the establishment of monitoring systems—saw rapid increases in both background concentrations and local production due to extensive O_3 for-

mation. Annual synthesis analyses highlight that wind convergence is likely a significant factor in the heightened O_3 concentrations observed in Anhui and Northwest Jiangsu. Additionally, bioVOC emissions transported from western and southern mountainous regions substantially influence O_3 levels in Hefei, Ma@anshan, Wuhu, and Nanjing, while ozone transport to Shanghai is closely linked with prevailing southwest winds and southerly breezes. During years of high local generation, elevated temperature anomalies align with O_3 production patterns, underscoring the strong positive correlation between the temperature and ozone formation.

(3) Using the TOR methodology, mutual transport contributions among forty-two cities within the YRD are estimated to range between 45.2% and 65.1%, indicating that transported contributions to ozone levels generally exceed those from local generation. Specifically, for the four focal cities, Shanghai shows significant transmission impacts, with contributions exceeding 50%, while Hangzhou experiences minimal transport impacts at under 20%. The TOR method effectively quantifies air pollution transport rates by combining ground-level measurements with wind field data, addressing uncertainties in inter-regional pollutant transport caused by wind field fluctuations. This approach provides an improvement over previous methodologies by accurately characterizing pollutant transfer dynamics across the YRD and distinguishing regional pollutant trajectories.

(4) The characteristics of ozone transport between cities in the Yangtze River Delta region are significant. From the perspective of key cities, some cities are affected by the main wind direction, while others have different transport distances. These differences are related to ozone pollution types and weather conditions and need further discussion.

Author Contributions: Conceptualization, J.M.; Methodology, Y.C., J.M. and X.W.; Validation, X.W.; Formal analysis, Y.C., J.M. and J.B.; Data curation, Y.C., J.M. and J.B.; Writing—original draft, Y.C.; Writing—review & editing, J.M.; Supervision, J.M.; Funding acquisition, J.M. All authors have read and agreed to the published version of the manuscript.

Funding: This research was supported by the National Natural Science Foundation of China (grant no. 42375067, 42075051, 42375056, and 42288101).

Institutional Review Board Statement: this statement if the study did not require ethical approval.

Informed Consent Statement: Informed consent was obtained from all subjects involved in the study.

Data Availability Statement: The datasets generated and/or analysed during the current study are not publicly available due to the data used is not public and is huge. but are available fromthe corresponding author on reasonable request.

Conflicts of Interest: The authors declare no conflict of interest.

References

1. Zhan, Y.; Luo, Y.Z.; Deng, X.F.; Grieneisen, M.L.; Zhang, M.H.; Di, B.F. Spatiotemporal prediction of daily ambient ozone levels across China using random forest for human exposure assessment. *J. Environ. Pollut.* **2018**, *233*, 464–473.
2. Li, M.; Zhang, Q.; Kurokawa, J.-I.; Woo, J.-H.; He, K.; Lu, Z.; Ohara, T.; Song, Y.; Streets, D.G.; Carmichael, G.R.; et al. MIX: A mosaic Asian anthropogenic emission inventory under the international collaboration framework of the MICS-Asia and HTAP. *J. Atmos. Chem. Phys.* **2017**,*17*, 935–963.
3. Yang, J.; Bu, D.; Liu, J.;Du M. A Review of the Current Status of Urban Ozone Pollution Prevention and Control in China. *J. Environ. Sustain. Dev.* **2022**, *4*, 86–90.
4. Zhao, Y. Characteristics of Ozone Pollution and Source Apportionment of VOCs in Typical Cities of the Yangtze River Delta Region. *J. Environ. Sci. Res.* **2024**, *37*, *1500*–1512. https://doi.org/10.13198/j.issn.1001–6929.2024.05.09.

5. Wang, Q. Characteristics of VOCs Variations and Their Contribution to O_3 Pollution in the Summer of Shanghai® Suburbs. *J. Environ. Sci.* **2023**, *45*. https://doi.org/10.13227/j.hjkx.202307220.
6. Li L.; Xu J.; An J.Y; Huang C.; Zhu S.H.; Zhou M.; Li X.M. The air pollution issues under the economic and energy constraint and their implications on the regional joint-effort in the Yangtze River Delta region. *J. China. J. Environ. Manag*. **2017**, *9*, 9–18. http://zghjgl.ijournals.cn/ch/reader/view_abstract.aspx?file_no=20170504&flag=1
7. Sun L.; Zhang H.; Wang H.B.; Wei Y.W.; Temporal and Spatial Distribution of Ozone in Typical Cities of Yangtze River Delta Region and Its Correlation with Meteorological Factors. *J. Atmos. Environ. Optics*. **2021**, *16*, 483–494
8. Wang, Y.; Zhu, S.; Ma, J.; Shen, J.; Wang, P.; Wang, P.; Zhang, H. Enhanced atmospheric oxidation capacity and associated ozone increases during COVID-19 lockdown in the Yangtze River Delta. *J. Sci. Total Environ.* **2021**, *768*, 144796.
9. Lin, W.; Guo, X. Spatial and temporal distribution characteristics of ozone in urban agglomerations in China. *J. China Environ. Sci.* **2022**, *42*, 24812494.
10. Fan, Q.; Liu, Y.; Wang, X.; Fan, S.; Chan, P.W.; Lan, J.; Feng, Y. Effect of different meteorological fields on the regional air quality modelling over Pearl River Delta, China. *J. Int. J. Environ. Pollut.* **2013**, *53*, 3–23.
11. Zhang, Z.; Zhang, X.; Gong, D.; Quan, W.; Zhao, X.; Ma, Z.; Kim, S.-J. Evolution of surface O_3 and $PM_{2.5}$ concentrations and their relationships with meteorological conditions over the last decade in Beijing. *J. Atmos. Environ.* **2015**, *108*, 67–75.
12. Huang, X.-G.; Zhao, J.-B.; Cao, J.-J.; Song, Y.-Y. Spatial-temporal variation of ozone concentration and its driving factors in China. *J. Environ. Sci.* **2019**, *40*, 1120–1131.
13. Liu, J.; Wu, D.; Fan, S.J.; Deng, T. Influence of Precursors and Meteorological Factors on Ozone Pollution in the Pearl River Delta Region. *J. China Environ. Sci.* **2017**, *37*, 813–820.
14. Xie, F.J.; Lu, X.B.; Yang, F.; et al. Impact of Ozone Pollution Transport and Identification of Potential Source Regions during Spring and Summer 2017 in Nanjing Area. *J. Environ. Sci.* **2021**, *42*, 88–96.
15. Zhao, S.; Yu, Y.; Qin, D.; Yin, D.; Dong, L.; He, J. Analyses of regional pollution and transportation of $PM_{2.5}$ and ozone in the city clusters of Sichuan Basin, China. *J. Atmos. Pollut. Res.* **2019**, *10*, 374–385.
16. Liu, N.; Yu, Y.; Ma, X.Q. Seasonal Characteristics of Air Pollution Sources and Transport in Xining City. *J. Environ. Sci.* **2021**, *42*, 1268–1279.
17. Li, W.; Sheng, L.; Song, Z.X.; et al. Source Apportionment of Particulate Matter in February at Beijing National Olympic Sports Center Based on Multiple TSM Methods. *J. Meteorol. Mon.* **2020**, *46*, 687–694.
18. Potier, E.; Waked, A.; Bourin, A.; Minvielle, F.; Péré, J.C.; Perdrix, E.; Michoud, V.; Riffault, V.; Alleman, L.Y.; Sauvage, S. Characterizing the regional contribution to PM_{10} pollution over northern France using two complementary approaches: Chemistry transport and trajectory-based receptor models. *J. Atmos. Res.* **2019**, *223*, 1–14. https://doi.org/10.1016/ j. atmosres. 2019.03.002.
19. Nzotungicimpaye, C.M.; Abiodun, B.J.; Steyn, D.G. Tropospheric ozone and its regional transport over Cape Town. *J. Atmos. Environ.* **2014**, *87*, 228–238.
20. Vellingiri, K.; Kim, K.H.; Lim, J.M.; Lee, J.-H.; Ma, C.-J.; Jeon, B.-H.; Sohn, J.-R.; Kumar, P.; Kang, C.-H. Identification of nitrogen dioxide and ozone source regions for an urban area in Korea using back trajectory analysis. *J. Atmos. Res.* **2016**, *176–177*, 212–221.
21. Xue, L.K.; Wang, T.; Gao, J.; Ding, A.J.; Zhou, X.H.; Blake, D.R.; Wang, X.F.; Saunders, S.M.; Fan, S.J.; Zuo, H.C.; et al. Ground-level ozone in four Chinese cities: Precursors, regional transport and heterogeneous processes. *J. Atmos. Chem. Phys.* **2014**, *14*, 13175–13188.
22. Wang, M.; Yim, S.H.; Wong, D.; Ho, K. Source contributions of surface ozone in China using an adjoint sensitivity analysis. *J. Sci. Total Environ.* **2019**, *662*, 385–392. https://doi.org/10.1016/j.scitotenv.2019.01.116.
23. Wang, P.; Chen, Y.; Hu, J.; Zhang, H.; Ying, Q. Source apportionment of summertime ozone in China using a source-oriented chemical transport model. *Atmospheric Environ.* **2019**, *211*, 79e90. https://doi.org/10.1016/j.atmosenv.2019.05.006.
24. Kalnay, E.; Kanamitsu, M.; Kistler, R.; Collins, W.; Deaven, D.; Gandin, L.; Iredell, M.; Saha, S.; White, G.; Woollen, J.; et al. The NCEP/NCAR 40-year reanalysis project. *J. Bull. Am. Meteorol. Soc.* **1996**, *77*, 437–471.
25. Nielson-Gammon, J.; Tobin, J.; Mcneel, A.; Li, G. *A Conceptual Model for Eight-Hour Ozone Exceedances in Houston, Texas Part I: Background Ozone Levels in Eastern Texas*; Texas A&M University: College Station, TX, USA, 2005.
26. Stein, A.; Draxler, R.R.; Rolph, G.D.; Stunder, B.J.B.; Cohen, M.D.; Ngan, F. Noaa® hysplit atmospheric transport and dispersion modeling system. *J. Bull. Am. Meteorol. Soc.* **2015**, *96*, 2059–2077.
27. Shneiderman, B. The Eyes Have It: A Task by Data Type Taxonomy for Information Visualizations. In Proceedings of the 1996 IEEE Symposium on Visual Languages, Boulder, CO, USA, 3–6 September 1996; pp. 336–343.
28. Seinfeld, J.H. Urban air pollution:state of the science. *J. Sci.* **1989**, *243*, 745–752.

29. Draxler, R.R.; Hess, G.D. *Description of the HYSPLIT-4 Modeling System*; NOAA Technical Memorandum ERL ARL-224; NOAA Air Resources Laboratory: Silver Spring, MD, USA, 1997; pp. 1–24.
30. Cao, Y.; Qu, Y.H.; Ma, J.H. Classification of ozone pollution and analysis of meteorological factors in the Yangtze River Delta. *J. Big Earth Data* **2023**, *7*, 318–337. https://doi.org/10.1080/20964471.2022.2157093.
31. Langford, A.O.; Senff, C.J.; Banta, R.M.; Alvarez, R.J., Sandberg, S.P.; Darby, L.S. Regional and local background ozone in Houston during Texas Air Quality Study 2006. *J. Geophys. Res. Atmos.* **2009**, *114.* https://doi.org/10.1029/2008JD011687.
32. Liang, Y.; Liu, Y.H.; Wang, H.; Li, L., Duan, Y.; Lu, K. Regional characteristics of ground-level ozone in Shanghai based on PCA analysis. *J. Acta Sci. Circumstantiae* **2018**, *38*, 3807–3815.
33. Wu, L.; Xue, L.K.; Wang, W.X. Review on the observation-based methods for ozone air pollution research. *J. Earth Environ.* **2017**, *8*, 479–491.
34. Shu, L.; Wang, T.J.; Han, H. Summertime ozone pollution in the Yangtze River Delta of eastern China during 2013–2017: Synoptic impacts and source apportionment. *J. Environ. Pollut.* **2019**, *257*, 113631.